

Measurement of weld joint parameters and their mathematical modelling

D. Novák^{1,*}, P. Kvasnová¹, J. Volf² and V. Novák²

¹Matej Bel University, Faculty of Natural Sciences, Department of Technology, Tajovského 40, SK974 01 Banská Bystrica, Slovakia

²Czech University of Life Sciences Prague, Faculty of Engineering, Kamýcká 129, CZ165 21 Prague, Czech Republic

*Correspondence: daniel.novak@umb.sk

Abstract. The article deals with verifying of weld quality of weld joints created by laser beam welding technology, primarily in agricultural components such as reel screws. We presents both metallographic check of the weld structure using electron microscopy, RTG-microanalysis and micro hardness measurement as well as used mathematical models of the welding process and respective weld joints geometry.

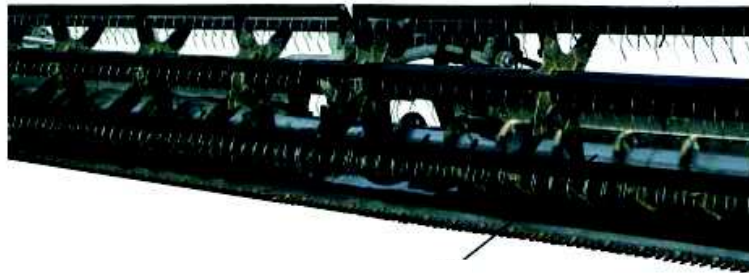
First the laser beam welding technology and concerned agricultural components are introduced. Further we specify individual steel types as well as laser types and we define specific welding parameters used in our measurements. We selected several samples of weld joints, which are further examined them in detail using optical microscopy, micro hardness measurements and RTG microanalysis. We further determined the weld shape, measured dimensions of individual weld joints as well as we checked the weld joints structure.

We further introduced a mathematical model based on the program ANSYS. The model can simulate temperatures, speed field and tensions within the weld joint, basing on known thermal conductivity of the base material and specified welding conditions. Using the model, we can predict the shape of the weld and the temperatures within the material. Finally, individual welding parameters and obtained weld joint samples are briefly discussed and the applicability of the model is evaluated.

Key words: steel, mathematical modelling, screw, laser welding, metallographic check.

INTRODUCTION

The scope of our research is to simulate the welding process using a mathematical model and to verify the weld joint parameters of selected stainless steels used in a reel in a combine harvester. Given the high cutting speed, this particular part requires high quality steel material and also high weld quality to guarantee the required toughness and sharpness of the components. A reel with the screw and its position are depicted in Fig. 1 and it is labelled with (1).



1

Figure 1. Reel with a screw (1).

Simulation represents imitation of the real things, states, relationships and processes. Its advantages include quick verification of systems' behaviour and detecting of potential problems and specific restrictions. It all leads to cost savings in the areas of use. The disadvantages of simulation are higher initial costs and a simplified approach. We created computer models of the weld joints using the simulation program ANSYS. This way we simulate the weld joints using temperature fields and we compare the simulation with the visual analysis of the welds.

To evaluate the structure of welded joints, we performed a metallographic check by means of electron microscopy and micro hardness measurement as proposed by Tillová et al. (2011). We further performed RTG microanalysis to study the concentration of individual alloy elements across the material. Finally, we also created computer models of the weld joints using the simulation program ANSYS.

Screw

A screw is one of the oldest methods known to transport materials of various kinds. The use of screws applies extensively, either attached to a machine as a combined harvester, mill, filter, metering device for feeding poultry and livestock. Or they are used as a separate screw conveyor. The screw is capable of transporting all kinds of loose, granular or granular materials, and even fluids. For the construction of reels are used high-quality materials such as aluminium and stainless steels, associated with robust mechanics and top hydraulic systems, for more information see Krupička & Rybka (2016).

Effective use of screws includes improved flow of the crop from the entire reel, its smooth flow to the trashing mechanism and minimizing of losses in the cutter bar, as stated by Pečenka & Hoffmann (2015) and Čedík et al. (2016).

Laser welding technology

Laser welding is a relatively complicated technological process, which includes several co-acting physical phenomena. The basic process of laser welding is a heat cycle that includes following steps: heating of welded materials, their melt, mixing the meltage in the weld bath and subsequent solidification of the meltage. The quality of steel material itself and weld joints affects also the structure stability, i.e. to resistance to external effects, such as temperature, pressure, corrosion and others, as discussed by Novotný et al. (2015; 2016).

Laser beam welding belongs – together with plasma and electron beam welding methods – to new, special melt welding methods. Their basic common features include a significant reduction of thermal energy consumption, which is achieved by increasing the energy density on the impact surface. If the surface energy density reaches value higher than 10^5 W cm^{-2} , the welded material heats rapidly above its boiling point and a cavity is being formed – a capillary tube, so called keyhole. The hole penetrates the material to a considerable depth, or even through its entire cross section.

The key features of laser beam welding processes include high temperature, high rate of heating and cooling and a strong concentration of power in a small space. These assumptions enable enhancing of the quality of welds compared to conventional methods; however, they expect use of advanced technology.

These features yield advantages like high welding accuracy, cleanness and possibility of operational automation. High heating rate limits the heat diffusion to the surroundings, which limits the transformation changes in the material. High density of power keeps the heat affected zone narrow that lowers tensions and deformations in the material. Other notable advantage of the laser welding method is so called remote welding, when the laser source may be placed up to 1.5 m from the welded object. This yields incomparable dynamics, limited only by the focusing speed. For more information about new welding technologies and more detailed description of their principles see Kubiček (2006) and Radek et al. (2014).

Various types of lasers used for the laser welding technology vary according to the environment from which the laser draws its energy. In our experiments we used three types of lasers: Nd:YAG, fibre and CO₂ laser. The energy for the laser beam is gained from the electron transition within an atom orbital of the active medium. A brief description of the used laser types gives the following summary:

- ✓ Nd:YAG: neodymium-doped yttrium aluminium garnet; Nd:Y₃Al₅O₁₂; crystal, the most used solid-state laser; infrared light with wavelength 1.064 μm.
- ✓ fiber: the active gain medium is an optical fibre doped with rare-earth elements, laser light is conducted by the fiber, the wavelength is determined by the doping element.
- ✓ CO₂: gas mixture from He + N₂ + CO₂ closed in a glass tube. Since its wavelength of 10.9 μm the beam cannot be conducted by optical fibres, mirrors have to be used.

MATERIALS AND METHODS

RTG microanalysis

RTG microanalysis is a method based on dispersion of X-rays, to obtain qualitative and quantitative data about the chemical composition of the studied material. We applied so called Line RTG microanalysis to study the concentration change of selected element across the sample. The measurements were performed at Slovak University of Technology in Bratislava, using Superprobe 733 spectrometer.

Welding parameters and steel composition

We modelled and subsequently checked several combinations of welding parameters as well as steel types. Following tables give the overview about the individual chemical composition of steels and they also state the exact welding parameters using various types of lasers.

Table 1 presents the chemical composition of Cr-Ni steels of types 17 246 (ISO X6CrNiTi18-10), 17 249 (ISO X2CrNi19-11) and 17 022 (ISO X20Cr13) determined by the RTG microanalysis.

Table 1. Chemical composition of used stainless Cr-Ni steels (average values)

Chemical element	Steel 17 246	Steel 17 249	Steel 17 022
C (%)	0.06	0.20	0.20
Cr (%)	18.5	16.5	11
Mn (%)	1	1	0.5
Ni (%)	9.5	9.5	-
Si (%)	0.5	0.35	0.5

Technical parameters, e.g. power, wavelength, focus distance etc. of all used laser types (CO₂, Nd:YAG and fiber) are stated Table 2.

Table 2. Technical parameters of used lasers

Laser type	Wavelength (μm)	Laser mode	Focus distance (mm)	Laser power (kW)	Welding gas	Gas flow (l.min ⁻¹)
Fiber	1.11	TEM00-Gaus	120	2.3	Ar	25
CO ₂	10.9	TEM00-Gaus	100	4	Ar	25
Nd:YAG	1.064	TEM00-Gaus	127	3.7	Ar	12

We further designed a variety of different welding parameters of Cr-Ni steels by given laser types. The proposed welding parameters presented in Table 3.

Table 3. Individual welding parameters

Laser type	Material (thickness)	Power (kW)	Welding speed (m min ⁻¹)	Focusing
Fiber	Steel 17 246 (2.5 mm)	2,3	3; 5; 8	0; +2; -2; -4
Nd:YAG	Steel 17 246 (2.5 mm)	1; 2,3; 3	3; 5; 8	0
CO ₂	Steel 17 249 (5 mm)	3,7	1,2; 1,8; 2,4; 3,0	0; -1
CO ₂	Steel 17 022 (5 mm)	3,7	1,2; 1,8; 2,4; 3,0	0; -1

RESULTS AND DISCUSSION

RTG microanalysis

First present the results of line RTG microanalysis, by means of which we analyse the concentration course of selected alloy elements within the steel. Fig. 2 presents the RTG microanalysis of all used steel types.

The graph presents the concentration change of selected alloy elements across the steel sample. Despite one peak of Si concentration (steel 17 246) there is no change that exceeds normal fluctuations of the alloy element concentration.

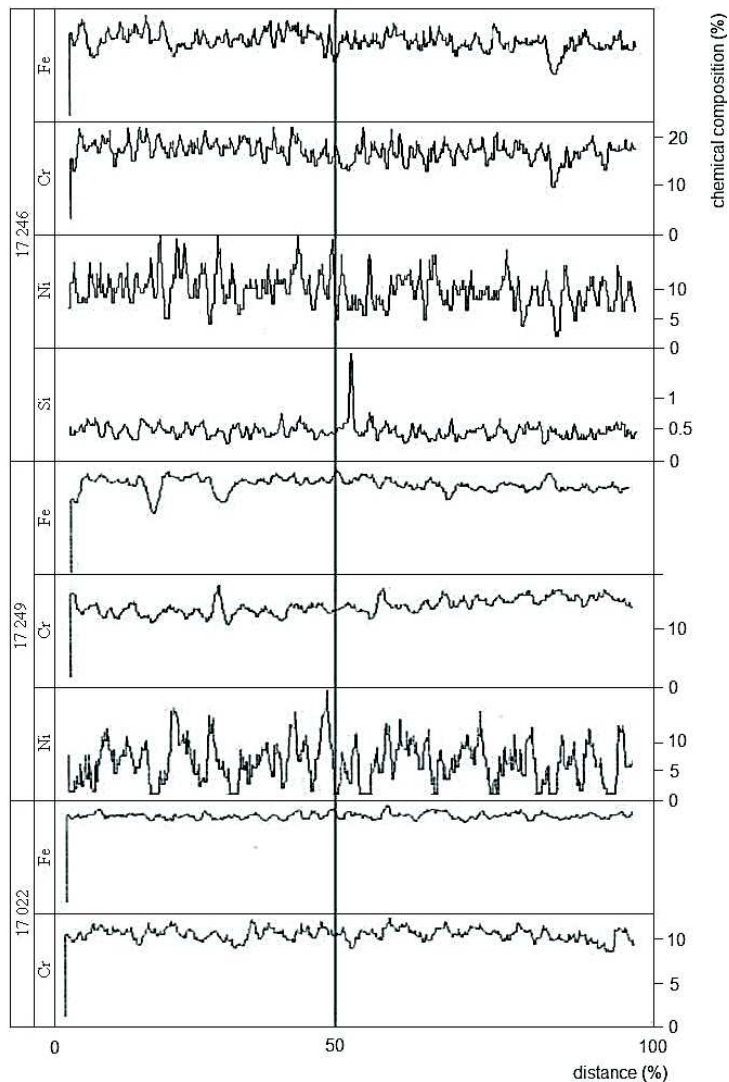


Figure 2. RTG microanalysis across the sample of steel types 17 246 (fiber laser), 17 249 and 17 022 (CO₂ laser).

Metallographic check

We further performed a metallographic check using electron microscopy, and micro hardness measurement, for further detail about these methods see Kardas (2013) and Meško et al. (2014). The macrostructure of the welds was assessed by electron microscope Carl Zeiss Axio A1M using software Proimage 4 at Technical University München. In total 29 individual samples of Cr-Ni steel 17 246, welded by fiber and Nd:YAG laser and Cr-Ni steels 17 249 and 17 022, welded by CO₂ laser have been prepared and analysed. In following Figs 3–6 we present eight selected pictures of the weld macrostructure from different steel types; individual geometrical parameters of the samples are given by Table 4.

Table 4. Parameters of steel samples

Sample No.	Steel	Laser type	Power (kW)	Welding speed (m.min ⁻¹)		Focusing	Weld depth (mm)	Weld area (mm ²)
1	17 246	fiber	2.3	3	0		2.5	1.8
2	17 246	fiber	2.3	5	-2		2.5	1.3
3	17 246	Nd:YAG	3	5	0		2.3	1.7
4	17 246	Nd:YAG	2.3	8	0		1.1	1.2
5	17 249	CO ₂	3.7	2.4	0		4.5	3.2
6	17 249	CO ₂	3.7	3	-1		3.3	2.4
7	17 022	CO ₂	3.7	3	-1		4	2.7
8	17 022	CO ₂	3.7	1.2	0		5.2	5.1

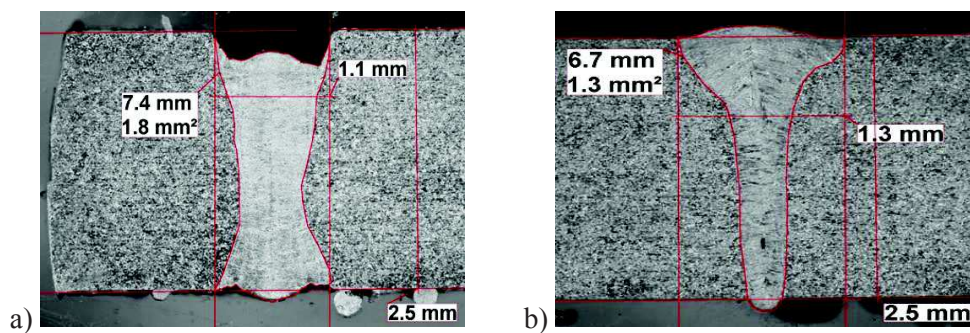


Figure 3. Weld macrostructure. Steel 17 246, fiber laser. Sample 1 (a) and sample 2 (b).

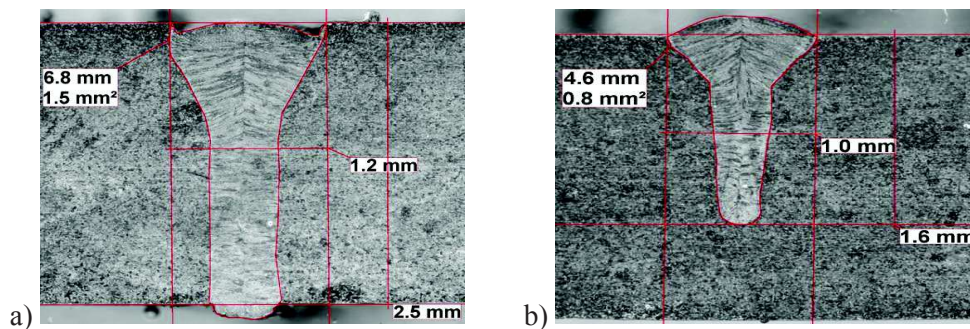


Figure 4. Weld macrostructure. Steel 17 246, Nd:YAG laser. Sample 3 (a) and sample 4 (b).

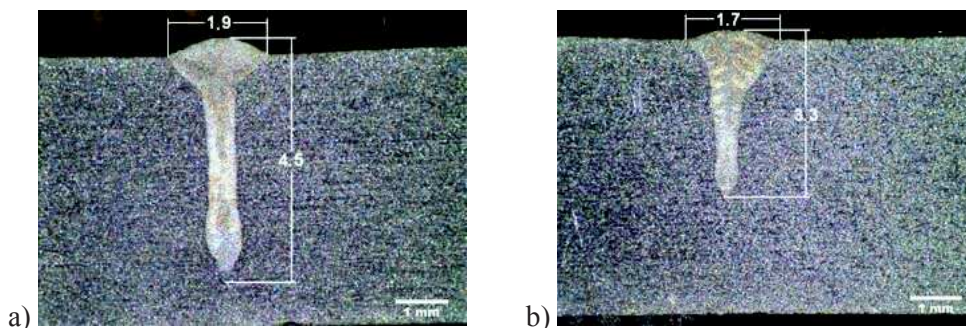


Figure 5. Weld macrostructure. Steel 17 249, CO₂ laser. Sample 5 (a) and sample 6 (b).

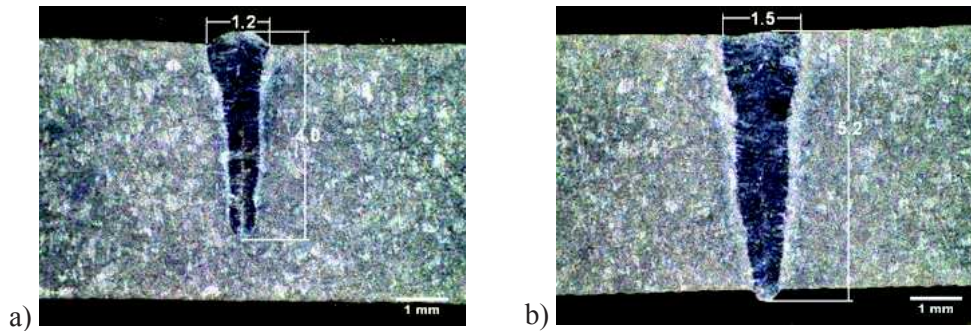


Figure 6. Weld macrostructure. Steel 17 022, CO₂ laser. Sample 7 (a) and sample 8 (b).

The weld geometry is affected by the combination of all welding parameters, i.e. laser type, power, welding speed and focusing. Notable are also shape similarities within one material, compare samples No. 5 and 6 with No. 7 and 8. All the prepared samples exhibit typical high depth-width-ratio, with narrowest weld parts below one millimetre. There is also a notable impact of negative values of laser focusing on the decreasing width and depth of the weld; however, to prove this we would need a dedicated experiment. As the heat flux of 2.3 to 3.7 kW is concentrated on the area of units of square millimetres (depending on the focusing), the welds' area is very small, between 1–5 mm².

Micro hardness measurement

Finally, there was also performed micro hardness measurement to determinate the hardness in the cross section of the welded area. The measurement was carried out using Vickers hardness test according to STN EN ISO 6507-1 (load of 100 g, load time 10 s) by means of optical NEOPHOT 21 metalgraph microscope.

The scheme of the micro hardness measurement is depicted in Fig. 7; the hardness was measured in 7 points in the transverse direction along the black bold line in the scheme with highlighted special points (weld, weld boundary, heat affected zone). The course of the hardness in the cross section of three selected samples from different steel types is graphically depicted in Figs 8–10; corresponding data are also presented in Table 5.

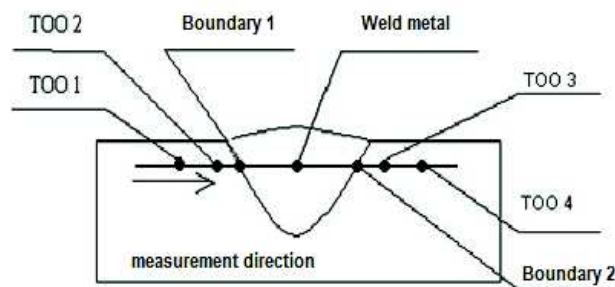


Figure 7. Micro hardness measuring scheme.

Table 5. Measured hardness of 17 246, 17 249 and 17 022 steel types

Point	HV, sample 1	HV, sample 5	HV, sample 8
TOO1	262	203	198
TOO2	254	207	204
Boundary 1	230	210	335
Weld	262	230	543
Boundary 2	238	210	336
TOO3	245	206	206
TOO4	254	203	198
Standard deviation	11.25	8.64	119.23

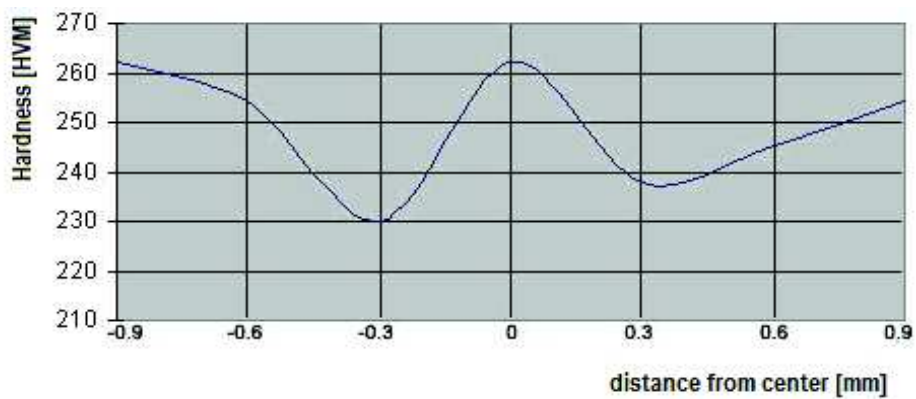


Figure 8. Course of hardness in cross section, sample 1 (steel 17 246).

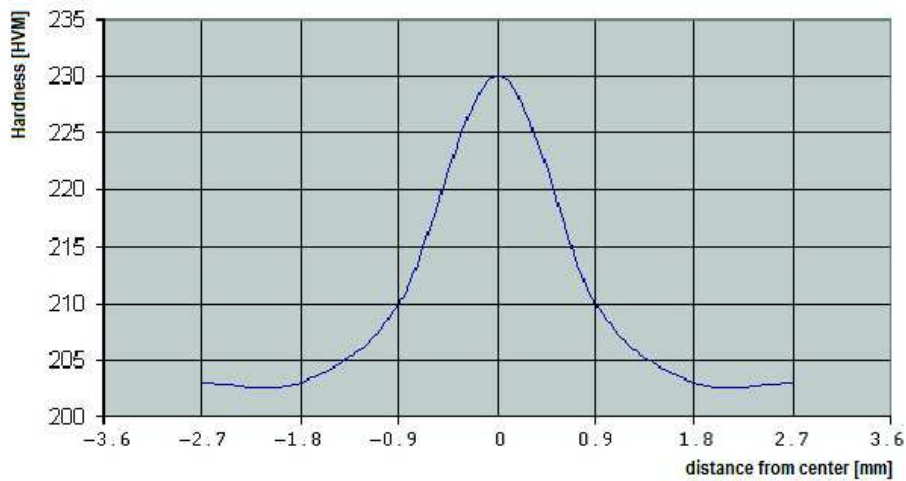


Figure 9. Course of hardness in cross section, sample 5 (steel 17 249).

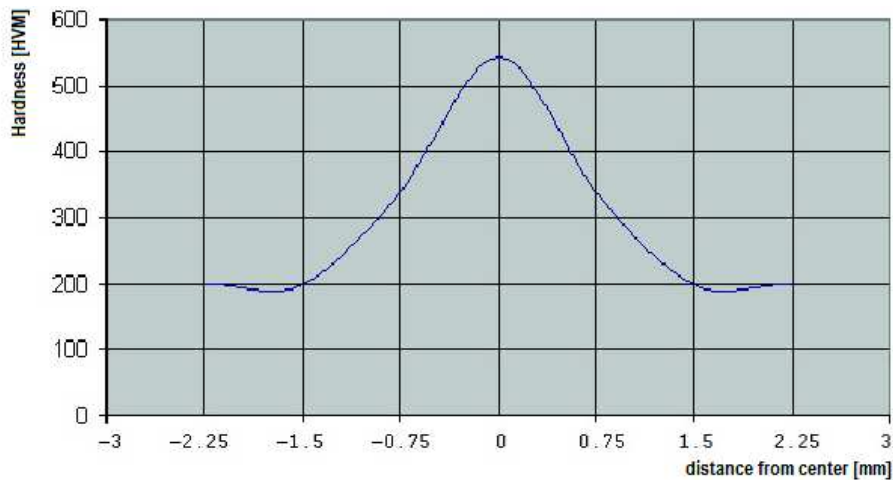


Figure 10. Course of hardness in cross section, sample 8 (steel 17 022).

The course of the hardness across the welded area is different for individual steel types. The hardness of steel 17 246 (Fig. 8) in the centre of the weld is about the same as of the base material; on the boundary of the weld the hardness drops of cca. 10%. In case of steel 17 249, the hardness in the middle of the weld is about 10% higher than of the base material (Fig. 9). However, due to the chemical composition and subsequent material changes during the welding process, the hardness of steel 17 022 is in the centre of the weld almost three times higher than the hardness of the base material. We can conclude that in one case there was observed 10% hardness drop compared to the base material; we do not consider this as a substantial degradation of the welded material. Compared to conventional welding technique, limited material degradation and narrow heat affected due to energy concentration into small area belong to prominent benefits of the laser welding technology.

Computer simulation

Finally we present the some pictures of the weld geometry and temperature fields using the program ANSYS, nearly described by Moravec et al. (2014) and Arslan et al. (2016). The scope of the modeling is to determine the effect of the moving laser beam across the material surface on the temperature field and to determinate the shape and geometry of the hat affected area. The simulation bases on the analysis of temperature and speed fields of the melt, which is considered as a dynamic fluid system. In the model, melted steel is assumed as incompressible fluid loaded by the heat flux from the laser beam.

The mathematical model of the weld was created for the steel type 17 246 (thickness 2.5 mm) and fiber laser (2.3 kW, welding speed 3 m min⁻¹, focusing +2). The exact thermo-physical and thermo-mechanical parameters of the steel used in the simulation are stated in Table 6.

Table 6. Simulation parameters; steel type 17 246

Thermal conductivity													
T [K]	293	473	673	873	1,073	1,273	1,473	1,673	1,873				
λ [W m ⁻¹ K ⁻¹]	15	17.3	20.05	22.85	25.6	27.9	30.2	32.6	35				
Mass heat capacity													
T [K]	293	473	673	873	973	1,173	1,273	1,473	1,673	1,723	1,823	1,873	
c_p [J kg ⁻¹ K ⁻¹]	469	472	477	515	540	600	632	696	760	770	760	745	
Density													
T [K]	293	373	473	673	873	1,073	1,273	1,473	1,673	1,873			
ρ [kg m ⁻³]	7,900	7,831	7,763	7,700	7,620	7,580	7,500	7,450	7,400	7,350			
Heat transfer coefficient													
T [K]	323	373	473	573	673	773	873	973	1,073	1,273	1,473	1,673	1,873
h [Wm ⁻² K ⁻¹]	13	17	23	30	38	49	63	79	99	150	217	305	357
Linear thermal expansion coefficient													
T [K]	293	373	473	673	873	1,073	1,273	1,473	1,673	1,873			
$\alpha_l \cdot 10^6$ [K ⁻¹]	16.8	17.2	17.5	18	18.5	19	19.4	19.8	20.1	20.3			
Young's modulus													
T [K]	293	373	473	673	873	1,073	1,273	1,473	1,673	1,873			
E [GPa]	200	195	187	172	157	135	50	26	15	5			
Yield strength													
T [K]	293	473	673	873	1,073	1,273	1,473						
R_e [MPa]	235	230	210	137	50	23	15						
Young's modulus (tangential)													
T [K]	293	473	673	873	1,073	1,273	1,473						
E_t [MPa]	1,185	1,160	938	690	250	120	30						

On basis of the thermal capacity and conductivity coefficients, we can create a base 2D model, which enables the analysis of temperature and speed fields of the material. The model assumes the dynamical viscosity of the meltage as function of temperature. The surface of the material is loaded by heat flux from the laser beam and by overpressure of 300 Pa in the axis of the laser beam with gaussian course; setting this condition is necessary to calculate the speed fields.

The temperature field is time variable and it determines the heat profile of the weld bath of the molten material under given material and parameters. The simulation of the temperature field in time $t = 0.018$ s from the welding start is depicted in Fig. 11; it shows the temperature distribution with color marked areas of specified teperature levels. The simulation of the temperature in dependency on time within selected positions of the weld is presented in following Fig. 12.

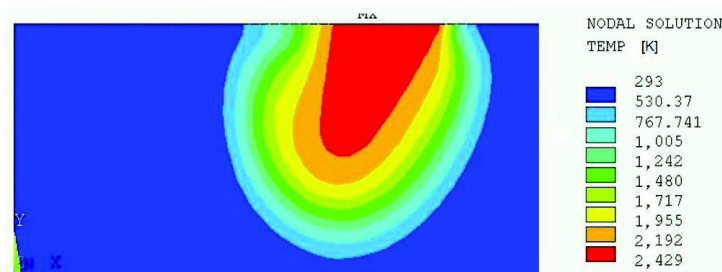


Figure 11. Simulation of the temperature field [K] in time $t = 0.018$ s from the welding start.

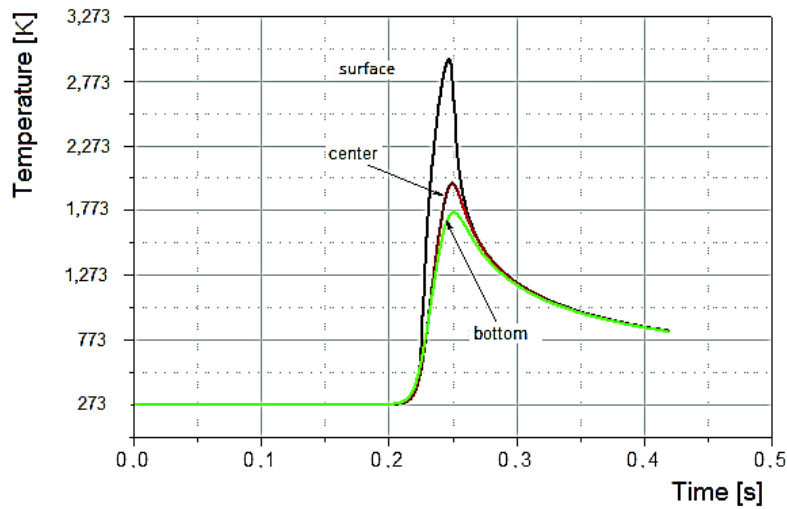


Figure 12. Time course of temperatures [K] in selected points.

In the previous figure, it is shown the time course of temperatures in the three nodes of the network model (surface, middle and bottom) with identical x-coordinate. It is apparent a rapid increase of temperature due to the laser beam effect and subsequent cooling due to conducting of the heat into the surrounding material, due to heat convection into the bypassing gas and due to radiation into the environment.

The final 3D model further enables to simulate non-stationary temperature fields and connected thermo-elastic and thermo-plastic tensions within the material, including residual (Mises) tensions. Hereby we need to set the stated material parameters as function of temperature. In the 3D model (see Fig. 13), calculated tensions can be displayed as 3D fields. Here the laser beam moves from the low left to the upper right corner. Prior to impact of the laser beam, there is a ‘tension wall’ with increased tension (red color). The tension vanishes under the passing laser beam (blue color – liquid state). After passing arises a field of increased tension, the residual tension.

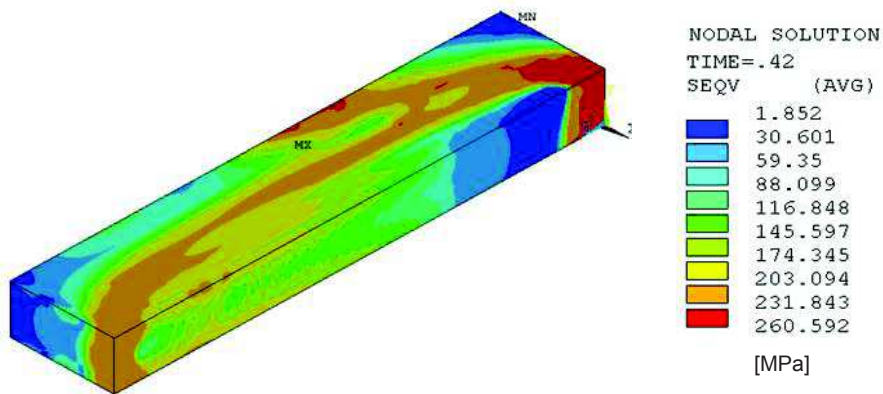


Figure 13. Tensions [MPa] under moving laser beam, $t = 0.42$ s.

The model of the geometrical profile of the weld in 3D-view can be seen in Fig. 14, where the boundary of the melted area is highlighted. The geometrical shapes of the boundary of the melted area obtained by the simulation are similar to the real shapes of the weld macrostructure under same conditions; see Fig. 15 with the real weld joint under the same welding parameters (steel 17 246, thickness 2.5 mm, fiber laser 2.3 kW, welding speed 3 m min⁻¹, focusing +2). The main issue when simulating the shape and dimensions of the weld joint is to specify exactly the material parameters, particularly its thermal conductivity. In order to near the real shapes, it is necessary to consider the welded part as orthotropic material and perform recalculations of its thermal conductivity.

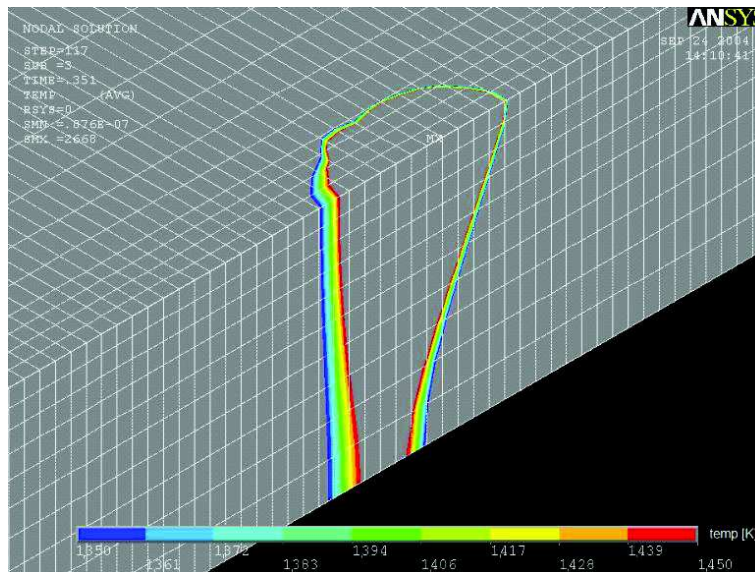


Figure 14. 3D view on the melted area boundary.

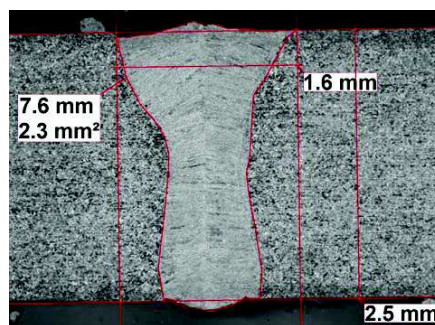


Figure 15. Weld macrostructure; steel 17 246, fiber laser.

CONCLUSIONS

Our research focuses on quality check and mathematical simulation of welds created by the laser welding technology. We prepared weld samples from several types of steels using different laser welding methods. We examined these samples using metallographic check by electron microscopy, micro hardness measurement and RTG-microanalysis. Hereby we obtained a detailed analysis of the welds. Using the above-described methods, we could determine the geometry of the weld, hardness and alloy concentration within the weld and surrounding area.

Using the laser welding technology, we measured in case of one sample only a 10% strength drop compared to the strength of the base material; other samples exhibit increase of strength in the weld area. Basing on the measurements of the weld geometry and structure, we proved the generally stated advantages of the laser welding technology, such as narrow heat affected zone, low deformations, high preciseness etc. The typical nail shape of the welds with high depth-with ratio was also observed; however, the final geometry of the weld joint depends not only on the laser parameters, but on the welded material, too. Further it has to be noted that the weld appearance change with focusing. Although we observed an impact of selected focus values on the weld geometry, a general prove would need a dedicated experiment.

Finally we presented a mathematical simulation of the welding process using the program ANSYS. Using the program we can simulate the temperature distribution within the weld, the temperature change in dependency on time, the geometrical shape of the weld and last but not least the residual tensions within the material. To simulate the thermal behaviour of the material exactly, it is necessary to set many material parameters (such as thermal conductivity and others), but it is also required to perform some recalculations with respect to real material characteristics. Fulfilling these conditions, the mathematical model is capable to simulate the real shape of the weld quite precisely; thus it makes use of the cost-saving effect of the simulation.

In further research, we would like to concentrate in detail on impact of laser focusing on the weld structure and geometry; as well as on the influence of used gases on the weld. We would also like to continue our work on increasing the accuracy of the mathematical model.

REFERENCES

- Arslan, S., Tursun, N., Kurtulmus, F. & Gülec, D. 2016. Use of thermal images for optimizing burner height, operating pressure, and burner angle of a weed flamer. *Agronomy Research* **14**(1), 14–24.
- Čedík, J., Pexa, M., Chyba, J., Vondrášek, Z. & Pražan, R. 2016. Influence of blade shape on mulcher blade air resistance. *Agronomy Research* **14**(2), 337–344.
- Kardas, E. 2013. The analysis of quality of ferrous burden materials and its effect on the parameters of blast furnace process. *Metallurgy* **52**(2), 149–152.
- Krupička, M. & Rybka, A. 2016. New design of roller separation line and its effect on the separation of hop mater. *Agronomy Research* **14**(2), 450–459.
- Kubiček, J. 2006. *Special methods of melt welding. Pressure welding*. VUT v Brně, Brno, Czech Republic (in Czech).

- Meško, J., Zrak, A., Mulczyk, K. & Tofil, S. 2014. Microstructure analysis of welded joints after laser welding. *Manufacturing technology* **14**(3), 355–359.
- Moravec, J., Bradáč, J. & Nováková, I. 2014. Ways of numerical prediction of austenitic grain size in heat-affected zone of welds. In: *7th International Conference on Innovative Technologies for Joining Advanced Materials*, TIMA 2014, Trans Tech Publications Ltd.
- Novotný, J., Honzík, J., Pilous, V. & Stránský, K. 2015. Properties of welded joints in Power Plant. *Manufacturing Technology* **15**(6).
- Novotný, J., Honzík, J., Pilous, V. & Stránský, K. 2016. Verification for the causes of the degradation of welded joints in power plant. *Manufacturing Technology* **16**(5), 1106–1110.
- Pečenka, R. & Hoffmann, T. 2015. Harvest technology for short rotation coppices and costs of harvest, transport and storage. *Agronomy Research* **13**(2), 361–371.
- Radek, N., Meško, J. & Zrak, A. 2014. Technology of laser forming. *Manufacturing technology* **14**(3), 428–431.
- Tillová, E., Chalupová, M., Hurtalová, L. & Ďurínková, E. 2011. Quality control of microstructure in recycled Al-Si cast alloys. *Manufacturing Technology* **11**, 70–76.